CrossMark

ORIGINAL ARTICLE

Validation of gridded data set of global surface wind/wind-stress vector field

Suguru Kameda[1] · **Kunio Kutsuwada**[1]

Abstract Gridded data of global surface wind/wind-stress vectors, called J-OFURO v2, were obtained from satellite scatterometer (QuikSCAT/SeaWinds) data for the decade from August 1999 to July 2009. The data were validated by comparing with (1) in situ measurements from moored buoy observations, (2) a data product from the same scatterometer using a different gridding procedure (IFRE-MER), and (3) data products based on numerical models (NCEP-1 and NCEP-2). The results on averaging all buoy data revealed lower mean differences, lower root-mean-square (RMS) differences, and higher correlations for the wind/wind-stress components for the J-OFURO v2 product than the other data products. The statistical values calculated for each buoy station showed tendencies of decreasing reliability with increasing latitude in the midlatitude region, while the reliabilities in the equatorial areas were low. We performed intercomparisons between the J-OFURO v2 data and the other data sets to clarify discrepancies among different wind products in open ocean regions with few moored buoys. We determined that the meridional wind components from the NCEP products exhibited poleward deviations compared to data from the J-OFURO v2 product. Relatively high mean differences, high RMS differences, and low correlations were found in the equatorial ocean for the NCEP products. Striped features were spatially correlated with buoy locations in the equatorial Pacific, which suggested that the reliability of the NCEP products was governed by buoy locations in this region.

Keywords QuikSCAT · Validation · Wind vector products · Data reliabilities

1 Introduction

Wind-stress vector fields have been used for calculations of volume transports in currents of the upper ocean based on the classical wind-driven ocean circulation theory (Sverdrup 1947). The signals of wind and wind-stress vectors are important physical elements for investigations of air–sea interactions (Xie 2004; Chelton et al. 2004; Small et al. 2008). More in-depth information is required for wind-stress vector fields of the sea surface and for various oceanic basins, and high reliability with regard to space and time is needed for investigating air–sea interactions.

A variety of data sets of surface wind/wind-stress vectors covering the global ocean and derived using different procedures are available to oceanographers and meteorologists. One of these data sets is wind data obtained from satellite measurements. Wind data measured using satellite-based microwave scatterometers can supply a wide range of homogeneous data for sea surface wind speed and wind direction and with relatively fast revisit time. We have constructed gridded data sets for various types of surface meteorological parameters based on satellite observations. The product is called the Japanese Ocean Flux Data Sets with Use of Remote Sensing Observations (J-OFURO), and it includes sea surface wind and wind-stress vectors (momentum flux), and heat flux components. Validation studies for this wind data set have been made using meteorological buoys, and the results have shown that the wind data

✉ Kunio Kutsuwada
kkutsu@scc.u-tokai.ac.jp

Suguru Kameda
Suguru.kameda.1984@gmail.com

[1] School of Marine Science and Technology, Tokai University, 3-20-1, Orido, Shimizu, Shizuoka 424-8610, Japan

set had a reliability similar to or higher than other data sets (Kubota et al. 2002; Tomita and Kubota 2005; Kutsuwada et al. 2004, 2009). Previous studies have used the data only for limited periods. Data from the satellite QuikSCAT (QSCAT) was used in the development of the J-OFURO wind products; the QuikSCAT mission ended in November 2009 at the same time as we had completed the development of our QSCAT/J-OFURO v2 product. Thus, we performed the validation for the data set for the entire period.

Global wind data sets have also been developed using numerical models. These reanalysis products were created by using a data assimilation method for numerical weather prediction models using currently available observation data. The reanalysis wind products have been used successfully by many researchers, because the products have no missing gridded data. However, previous studies have shown that the wind products have different reliabilities, possibly due to the discrepancies in modelling procedures (e.g., Kubota et al. 2002). Thus, we attempt to clarify the reliabilities for various types of wind products by comparing data sets covering the decade-long period of QSCAT measurements.

Another motivation for the validation study is related to known discrepancies in the curl of the wind-stress field. For example, Risien and Chelton (2008) have shown that there were differences in the surface wind-stress fields when using wind vector products from the QSCAT and the National Center for Environmental Prediction/National Center for Atmospheric Research (NCEP/NCAR) reanalysis program (NRA1). Aoki and Kutsuwada (2008) demonstrated that there were differences between the Sverdrup flows calculated from different wind data sets in the mid-latitude area of the North Pacific Ocean, indicating that the differences were likely caused by the use of different wind products. Sasaki and Nonaka (2006) and Sasaki et al. (2006) simulated a numerical experiment of the Hawaiian Lee Countercurrent (HLCC) using two different wind products, the QSCAT and NCEP reanalysis and pointed out that there were significant discrepancies between the two simulated oceanic fields. These results highlight the necessity for investigating dependencies of simulated fields on wind-stress fields.

In this study, we will focus on the reliabilities of typical gridded data sets of wind vectors covering the global ocean. For this purpose, we selected two numerical reanalysis products provided by NCEP/NCAR and NCEP/Department of Energy (DOE), called the NRA1 and NRA2, respectively. The former is one of the most popular global products and has been used for numerous approaches such as analyses of climatic variability and as input data for ocean general circulation models (OGCM). The NRA2 is the corrected version of NRA1. Additionally, we also used a global wind product provided by the Institut Français de Recherche pour l'Exploitation de la Mer (IFREMER). This

product was derived using different methods for the development of the gridded product, but using the same wind products from the QSCAT satellite as in our analysis.

In the first step of examining the products' reliabilities, we compared time series data for the different wind products with in situ measurements from moored buoys. These validations are limited in some regions with moored buoys, such as tropical and near-coastal regions. On the other hand, we need information on the reliabilities of wind products in other regions, especially the open ocean of the mid-latitude areas, because the wind governs oceanic transports in the subtropical regions. In the next step, we will examine and compare different wind products.

2 Data and procedures

2.1 Global data set for satellite-derived wind products

2.1.1 QSCAT/J-OFURO v2

Gridded products of surface wind/wind-stress vectors covering the global ocean have been developed using satellite scatterometer (QSCAT/SeaWinds) data and the weighted average method (Kutsuwada 1998; Kubota et al. 2002); the products are called J-OFURO (http://dtsv.scc.u-tokai.ac.jp/j-ofuro/index.html). We used the L2B12 (level-2) data products provided by NASA JPL PO.DAAC (ftp://podaac-ftp.jpl.nasa.gov/) to develop the data set. Gridded data were obtained by using the weighted average method based on Kutsuwada (1998), where the weighted average is applied to raw data within a radius of influence (300 km for zonal, 150 km for meridional direction and 36 h of time). This data set consists of gridded data with 1×1 degree resolution in the area covering 30°E–390°E and 60°N–80°S for daily and monthly observations from August 1, 1999 to October 31, 2009. In this study, daily data were used for the validations. The wind stress on the sea surface was calculated using the drag coefficient by Large and Pond (1981) for wind speed and direction data of swath data (level 2), and data was gridded using the weighted average method. In addition to using the rain flag for the L2B12v2 raw data (obtained from PO.DAAC and based on the new method), in version 2.0 of our data set (QSCAT/J-OFURO v2), we used only data with a rain probability of less than 10% based on our quality control procedure.

2.1.2 QSCAT/IFREMER

We also used another satellite-derived gridded product of surface wind/wind-stress vectors over the world ocean supplied by the IFREMER. This product is created using satellite scatterometer data (QSCAT/SeaWinds;

L2B12v2) (Bentamy et al. 1996, 2014) and is called QSCAT-IFREMER (IFREMER) (for more information, refer to the user manual at ftp://ftp.ifremer.fr/ifremer/cer-sat/products/gridded/mwf-quikscat/documentation/mut-wqscat.pdf).

The QSCAT/IFREMER product differs from the QSCAT/J-OFURO product in terms of grid size (0.5 × 0.5 degree grid), temporal resolution (daily, weekly, monthly), the drag coefficient for calculation of wind stress (Smith 1980), and the gridding method (optimum interpolation method using the variogram coefficient with 600 km and 30 km/h for wind component). We used only daily data for QSCAT/IFREMER, downloaded from ftp://ftp.ifremer.fr/ifremer/cersat/products/gridded/mwf-quikscat/.

This data set is based on an older version of the QSCAT L2B12v3 product (Fore et al. 2014). In this study, we compared the J-OFURO and IFREMER products to validate the effects of the construction method using the same version of the QSCAT L2B12v2 for both products, as well as the new version for the IFREMER product from ftp://ftp.ifremer.fr/ifremer/cersat/products/gridded/MWF/L3/QuikSCAT/Daily/.

2.2 Numerical weather prediction model (NWPM) data

2.2.1 NCEP/NCAR reanalysis 1

We also used data sets of global wind parameters derived from numerical weather prediction models (NWPMs). One of the data sets is based on the NCEP/NCAR reanalyses (NRA1), and details are described by Kalnay et al. (1996). The data set covers the global ocean (Global T62 Gaussian grid) with a temporal coverage of 6 h, daily, and monthly and ranging from the 1950s to present. In this study, daily data were calculated on the basis of 6-h data (from http://www.esrl.noaa.gov/psd/data/gridded/data.ncep.reanalysis.surface.html).

2.2.2 NCEP/DOE reanalysis 2

A second data set of global winds derived from NWPMs and originating from NCEP is the NCEP/DOE (NRA-2) reanalyses, and details are described by Kanamitsu et al. (2002). Note that the reliability of this data set is not necessarily greater than for NRA1. Thus, we used both data sets, NRA1 and NRA2. NRA2 covers the global ocean (Global T62 Gaussian grid) and has the same temporal coverage as NRA1. Daily data used in this study were calculated from 6-hourly data (from http://www.esrl.noaa.gov/psd/data/gridded/data.ncep.reanalysis2.surface.html).

## 2.3 In situ measurement data from moored buoy observations

In situ measurement data are required for validation of wind speed/wind-stress vector data sets. In this study, we used measurement data from moored buoys. The data were obtained from the National Data Buoy Center (NDBC) located near the coast of the USA, the Tropical Atmosphere Ocean (TAO) and the Triangle Trans-Ocean buoy Network (TRITON) located in the equatorial Pacific, the Prediction and Research Moored Array in the Atlantic (PIRATA) located in the equatorial Atlantic, and the Kuroshio Extension Observatory (KEO) located in the Kuroshio Extension region of the North Pacific. We did not use data from buoys located within 50 km of any coast because the data are not considered appropriate for our purpose of validating wind vectors. The excluded data were from NDBC buoys in the mid-latitude areas, consisting of five buoys on the west coast and three on the east coast of the North American Continent.

Sea surface wind speed is traditionally defined as 10-min averaged values at 10 m height above sea level. Wind speed based on the satellite scatterometer data also was derived at 10 m height above sea level under neutral, stable conditions and using the wind retrieval algorithm. On the other hand, buoy data are measured every hour (NDBC and PIRATA) or every 10 min at 2–5 m height above sea level. Therefore, under the assumption that the data should represent neutral and statically stable conditions, all buoy data were converted to a height of 10 m above sea level using the Liu–Katsaros–Businger (LKB) model (Liu et al. 1979; Fairall et al. 1999). The daily means were averaged for 12 o'clock (UTC) every day. Figure 1 shows the buoy arrays used in this study. When a buoy location differed from the grid point in the wind data sets, the data measured at the buoy were derived using linear interpolation.

2.4 Statistical parameters used in our comparison

Statistics used for the validation study included mean differences (bias), root-mean-square differences (random differences), and correlation coefficients. The mean difference (MD) describes the difference between the mean values, with a small magnitude indicating high reliability. The root-mean-square difference (RMSD) describes the reliability with regard to change over time occurring in the wind fields. This value reflects random error based on estimation values, with a small magnitude indicating high reliability. The correlation coefficient (R) describes the similarity with regard to changes occurring in the fields.

Fig. 1 Locations of mooring buoy station
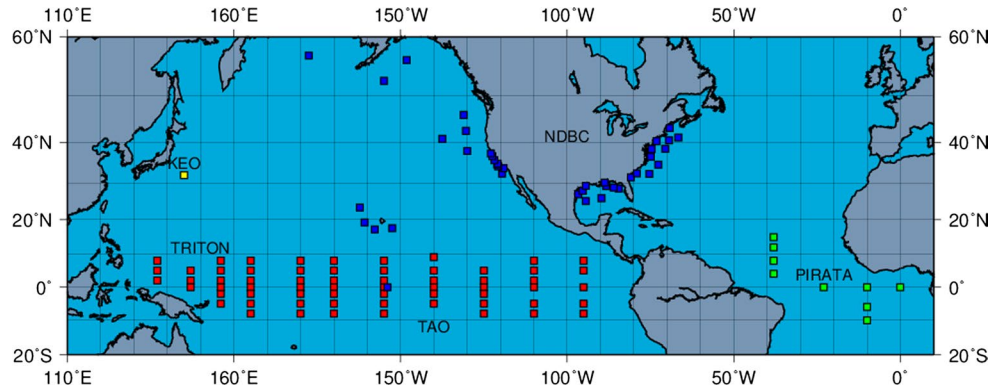
3 Validation of wind/wind-stress mean fields

3.1 10-year mean field

In this section, we describe basic features of the wind speed/stress vector fields for different data sets. Figure 2 shows the 10-year mean (from August 1999 to July 2009) wind vector field based on the QSCAT/J-OFURO v2, QSCAT/IFREMER, NRA1, and NRA2 products, depicted by length and direction of the arrows. These figures indicate that broad spatial features are similar for the data products. Some differences were observed in areas near boundary regions such as areas located between the trade and westerly wind regions and near-coastal regions. We expected that these differences in the wind distributions among the data products would result in differences in the wind-stress curl field. Specifically, we focused on
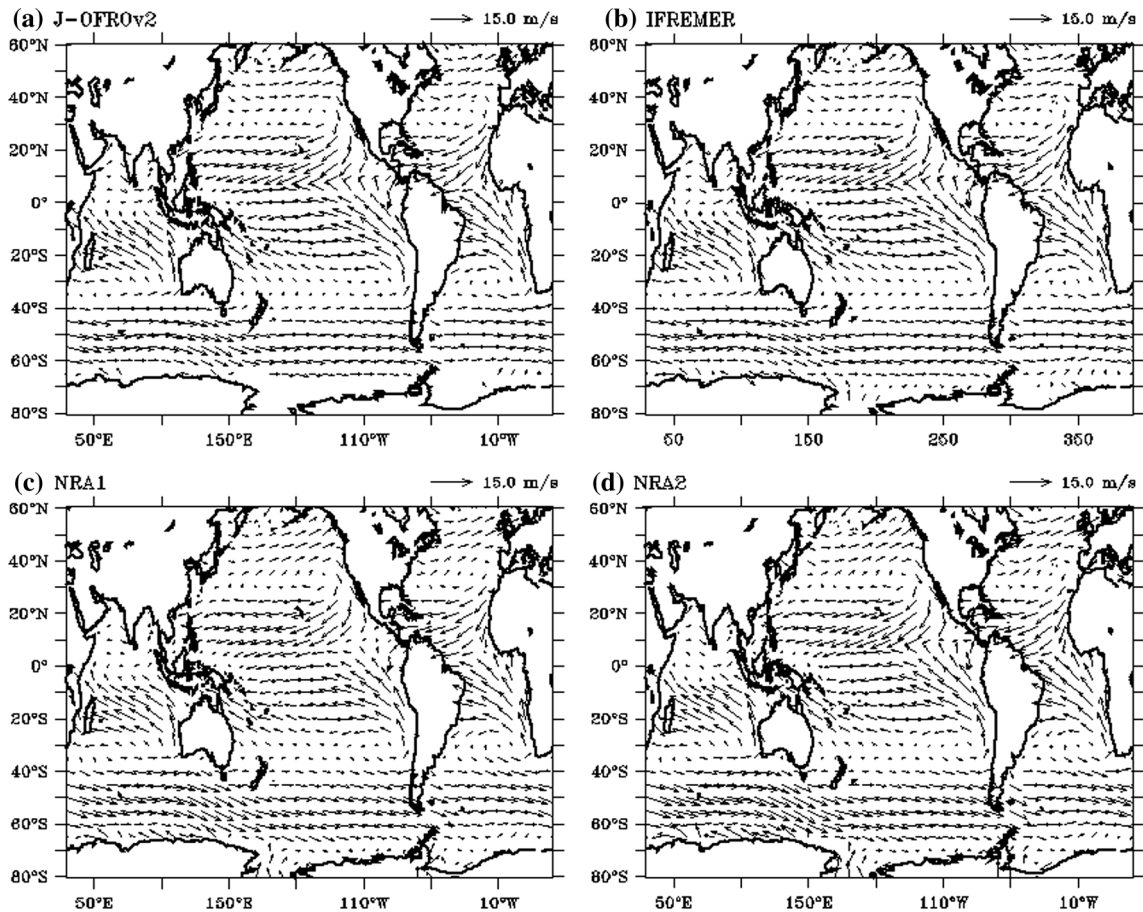
Fig. 2 Decadal mean fields of wind vector during 1999/8–2009/7. **a** J-OFURO, **b** IFREMER, **c** NRA1, **d** NRA2

the meridional gradient of the zonal wind stress which is important for calculations of the curl-τ field, because magnitudes of the zonal wind component were larger than for the meridional component.

Figure 3 shows meridional profiles for the zonal and meridional components of the wind speed/stress and the root-mean-square (RMS) for the 10-year mean from August 1999 to July 2009. There were discrepancies between the different data sets in latitudinal bands corresponding to the maxima/minima in the zonal components of mean wind speed/stress. The difference between the data sets was 0.5 m s^{-1} for the zonal wind speed and 0.05 N m^{-2} for the zonal wind stress. The differences occurred in the boundary region shown in the profile of the meridional component, specifically at the boundary between the northerly and southerly winds. The boundary was located at 45°N for the QSCAT data and 35°–40°N for the NCEP data.

The RMS profiles for the same period and for all data sets are shown in Fig. 3. Peak values in the RMS for the zonal wind (stress) were 1.3 m s^{-1} (0.028 N m^{-2}) and 1.7 m s^{-1} (0.050 N m^{-2}), respectively, and were located at 45°N and 45°S. Those peaks were related to the meridional movement of the westerly wind area. A large peak in the RMS for the zonal wind (stress) of 3.2 m s^{-1} (0.050 N m^{-2}) was located near 15°N. Maxima of RMS in the meridional wind were 1.8 m s^{-1} and occurred in a zone of 30°N–15°N for QSCAT, and were 2.1 m s^{-1} and occurred in a zone of 5°N–25°S for NCEP. These peaks relate to meridional movement in the trade wind region. In addition, the differences reached a maximum of 1.5 m s^{-1} for zonal wind

speed and 0.07 N m^{-2} for zonal wind stress in the Southern Ocean (50°S). With regard to the meridional component, differences between the J-OFURO v2 and IFREMER data and the reanalysis data (NRA1 and NRA2) were observed for all regions. In the Southern Ocean (50°S), the poleward anomalies in the reanalysis data from the satellite data reached a maximum of 1.0 m s^{-1} and 0.02 N m^{-2} for the meridional wind speed and stress, respectively. Those differences are known to affect calculations of wind speed and stress in the Southern Ocean (Wunsch 1998).

3.2 Validation of mean field by comparison with in situ measurements from moored buoy observations

In this subsection, we validate mean profiles of the data sets by comparison with measurements from moored buoy observations. Table 1 lists statistical values for the measurements from the meteorological buoy stations shown in Fig. 1. The statistical values (R, RMSD, MD) were calculated for a time series of 10 years from August 1, 1999 to October 31, 2009 using the following formulas:

$$\text{MD} = \frac{\sum_{i=1}^{n}(x_i - y_i)}{N} = \frac{1}{N}\left\{\left(\sum_{i=1}^{n} x_i\right) - \left(\sum_{i=1}^{n} y_i\right)\right\}, \quad (1)$$

$$\text{RMSD} = \sqrt{\frac{\sum_{i=1}^{n}\{(x_i - y_i) - \text{MD}\}^2}{N}}, \quad (2)$$
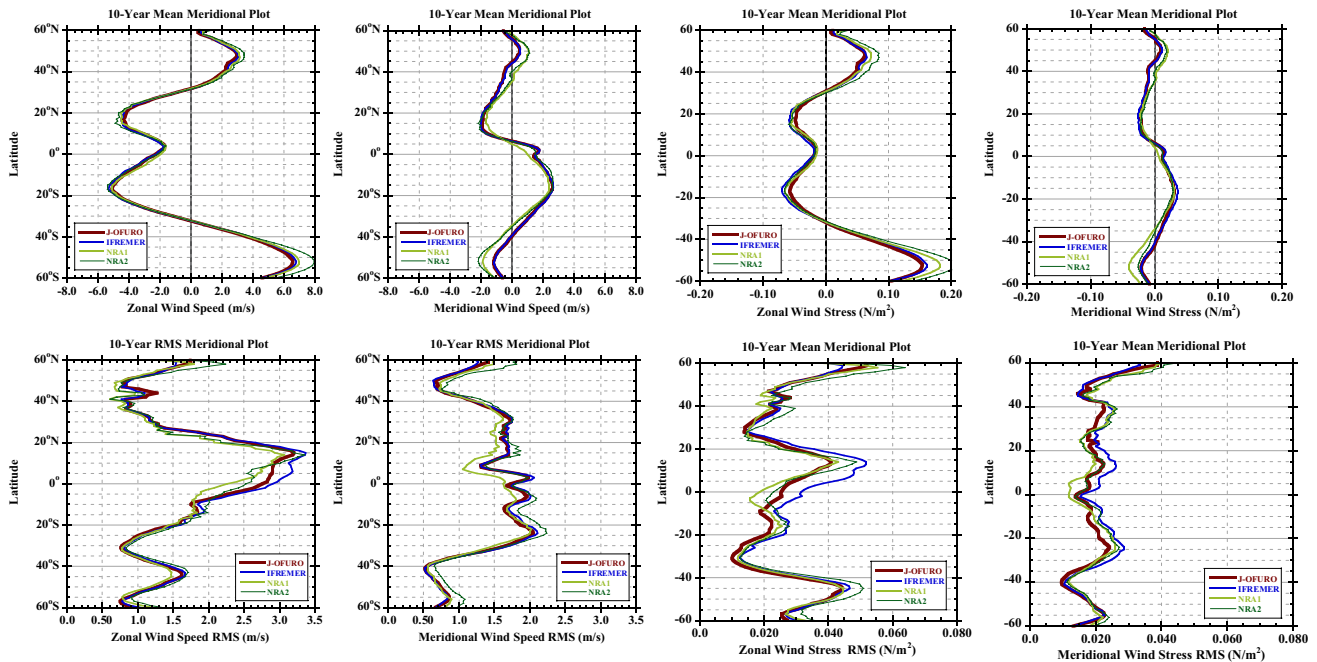
Fig. 3 Meridional profile of decadal mean (*upper*) and root-mean-square (RMS) (*lower*) by data sets and wind components

Table 1 Comparison of wind/wind-stress components for different wind products with in situ measurements by all buoy stations

	Zonal wind speed			Meridional wind speed			Number of data
	Correlation	RMSD	MD	Correlation	RMSD	MD	
QSCAT/J-OFUROv2	0.953	1.36	−0.03	0.936	1.33	−0.08	255300
QSCAT/IFREMER	0.928	1.78	−0.16	0.937	1.40	−0.05	255300
NRA1	0.932	1.64	0.34	0.877	1.81	−0.27	255300
NRA2	0.922	1.78	0.17	0.881	1.97	0.00	255300
	Zonal wind stress			Meridional wind stress			Number of data
	Correlation	RMSD	MD	Correlation	RMSD	MD	
QSCAT/J-OFUROv2	0.931	0.027	0.002	0.917	0.024	−0.001	255300
QSCAT/IFREMER	0.840	0.047	−0.004	0.905	0.029	−0.001	255300
NRA1	0.919	0.028	0.007	0.900	0.026	−0.002	255300
NRA2	0.910	0.030	0.005	0.899	0.028	0.000	255300

Table 2 Comparison of wind/wind-stress components for different wind products with buoy observations in the North Pacific (20°–40°N)

	Zonal wind speed			Meridional wind speed			Number of data
	Correlation	RMSD	MD	Correlation	RMSD	MD	
QSCAT/J-OFUROv2	0.912	1.95	0.16	0.909	1.78	−0.89	17,256
QSCAT/IFREMER	0.918	1.91	0.00	0.914	1.85	−0.92	17,256
NRA1	0.891	2.16	−0.09	0.892	1.91	0.18	17,256
NRA2	0.867	2.49	0.12	0.896	1.97	−0.10	17,256
	Zonal wind stress			Meridional wind stress			Number of data
	Correlation	RMSD	MD	Correlation	RMSD	MD	
QSCAT/J-OFUROv2	0.886	0.039	−0.001	0.892	0.036	−0.007	17,256
QSCAT/IFREMER	0.891	0.039	−0.001	0.886	0.044	−0.013	17,256
NRA1	0.885	0.039	−0.006	0.886	0.037	0.006	17,256
NRA2	0.849	0.044	−0.005	0.876	0.039	0.007	17,256

$$R = \frac{\sum\limits_{i=1}^{n} (x_i - \bar{x})(y_i - \bar{y})}{\sum\limits_{i=1}^{n} \sqrt{(x_i - \bar{x})^2} \sum\limits_{i=1}^{n} \sqrt{(y_i - y)^2}}. \qquad (3)$$

Note that RMSD is the random difference from which mean difference is removed.

Table 1 shows that the J-OFURO product had lower MD values for many components than the other data sets, except for the meridional wind and stress for the NRA2 product.

In the next step, we will describe spatial dependencies for these statistics. Table 2 lists the statistical values from buoy observations in the North Pacific (NDBC and KEO; 20–40°N). In this table, the J-OFURO product had higher MD values for many components compared to the other data sets. The statistical values calculated from buoy

observations in the equatorial Pacific (TAO/TRITON; 9°N–8°S) showed that the J-OFURO product had lower MD values than the other data sets (Table 3). Figure 4 shows scatter plots of the MDs for four wind and wind-stress products at all buoy stations for latitudes. Some of the results depicted in Fig. 4 are not consistent with the results shown in Tables 2 and 3. For example, the meridional wind components for the NCEP products have relatively low MD values in Table 2, while they have positive and negative values in Fig. 4. This indicated that large MD values with different signs canceled each other out, affecting the calculation of the average (Tables 1 and 2). This issue occurred for the NRA2 product in the equatorial zone. On the other hand, in the mid-latitude region (30°N–40°N) of the North Pacific (Table 2), the zonal and meridional components of wind speed/stress had larger MDs for the J-OFURO v2 and IFREMER products than for the NRA1 and NRA2

Table 3 Comparison of wind/wind-stress components for different wind products with TAO/TRITON buoy observations

	Zonal wind speed			Meridional wind speed			Number of data
	Correlation	RMSD	MD	Correlation	RMSD	MD	
QSCAT/J-OFUROv2	0.947	1.20	−0.10	0.936	1.08	0.05	144,865
QSCAT/IFREMER	0.896	1.78	−0.28	0.928	1.17	0.07	144,865
NRA1	0.913	1.56	0.49	0.786	1.88	−0.40	144,865
NRA2	0.895	1.66	0.21	0.804	1.92	0.17	144,865
	Zonal wind stress			Meridional wind stress			Number of data
	Correlation	RMSD	MD	Correlation	RMSD	MD	
QSCAT/J-OFUROv2	0.943	0.016	0.003	0.932	0.012	0.000	144,865
QSCAT/IFREMER	0.745	0.047	−0.006	0.886	0.019	0.000	144,865
NRA1	0.891	0.023	0.011	0.807	0.021	−0.004	144,865
NRA2	0.863	0.024	0.006	0.812	0.020	0.000	144,865

products. Large positive and negative MDs for the zonal and meridional components were observed at a buoy station in the zone of 30°N–40°N (Fig. 4). This buoy station is located in a near-coastal region (53.3 km from land) at 33.75°N, 119.05°W. In this area, the satellite-based gridded wind data are considered to be less reliable because of a lack of satellite measurements over land and the short-period coastal phenomena. These noisy data may have had an impact on the MD values of the meridional wind components.

For the IFREMER product, we obtained negative MDs greater than 1.0 m s^{-1} and 0.02 N m^{-2} for the zonal wind and wind-stress components, respectively (Fig. 4). Negative MDs were observed for the buoy stations at 2°N and 8°N in the central equatorial Pacific. The time series for the buoy station located at 5°N, 180° in this area revealed that the wind direction changed with respect to the position of the trade wind (see Fig. 8b in Sect. 4.1).

Additional differences were observed for the NRA1 product in the equatorial region. We observed negative MDs greater than 1.0 m s^{-1} and 0.02 N m^{-2} for the meridional wind and wind stress, respectively, in the northern hemisphere (0°–10°N), and positive MDs greater than 1.0 m s^{-1} and 0.02 N m^{-2} for the zonal wind and wind stress, respectively, in the southern hemisphere (0°–10°S) (Fig. 4). These features were not observed for any other product.

3.3 Comparison of mean fields derived from QSCAT/J-OFURO v2 and other data products

In order to verify the results for buoy comparisons in the previous section, we calculated the mean differences (MD) for the wind/wind-stress components between the QSCAT/J-OFURO v2 product and the other products

(Fig. 5). Large MDs were detected in the equatorial zone (between 20°N and 20°S) and in the westerlies zone (over 40°N/S), showing that those features depended on latitude. This suggested that the differences between the data sets were related to the cores of the westerly and the trade winds regions, and were caused by the differences in resolvability of the phenomena, associated with grid sizes for the data sets.

We found positive MDs for the meridional wind components derived from the NRA1 and NRA2 products in near-coastal regions (about 5° from the coast) on the west coast of North and South America. These features were related to the large negative MDs in the zone of 30°N–40°N for the QSCAT product (Fig. 4), because most of the buoy stations in the zone are located in near-coastal regions. It should be remembered that satellite wind products from microwave scatterometer data have less reliability in these regions because of sensor accuracy.

We also found relatively large values in the equatorial areas. For example, the zonal wind and wind stress for the IFREMER product had large negative MDs for buoy estimates located between 0° and 10°N (Fig. 4) and negative values in the central equatorial Pacific (150°E–110°W) (Fig. 5a, c). Note that the MD values for the zonal components were larger for the NCEP product than for the IFREMER product.

The zonal components from the NCEP product had positive values (greater than 1.0 m s^{-1} and 0.02 N m^{-2} for wind and wind stress, respectively) in the equatorial Pacific between 5°N and 5°S (Fig. 5e, g, i, k), while the meridional components had negative values (<-0.8 m s^{-1} and -0.02 N m^{-2}) between 0° and 5°N (Fig. 5f, h, j, l). In this zone, the meridional components from the NRA1 product had negative MDs for the buoy estimates greater than 1.0 m s^{-1} for wind and 0.02 N m^{-2} for wind stress
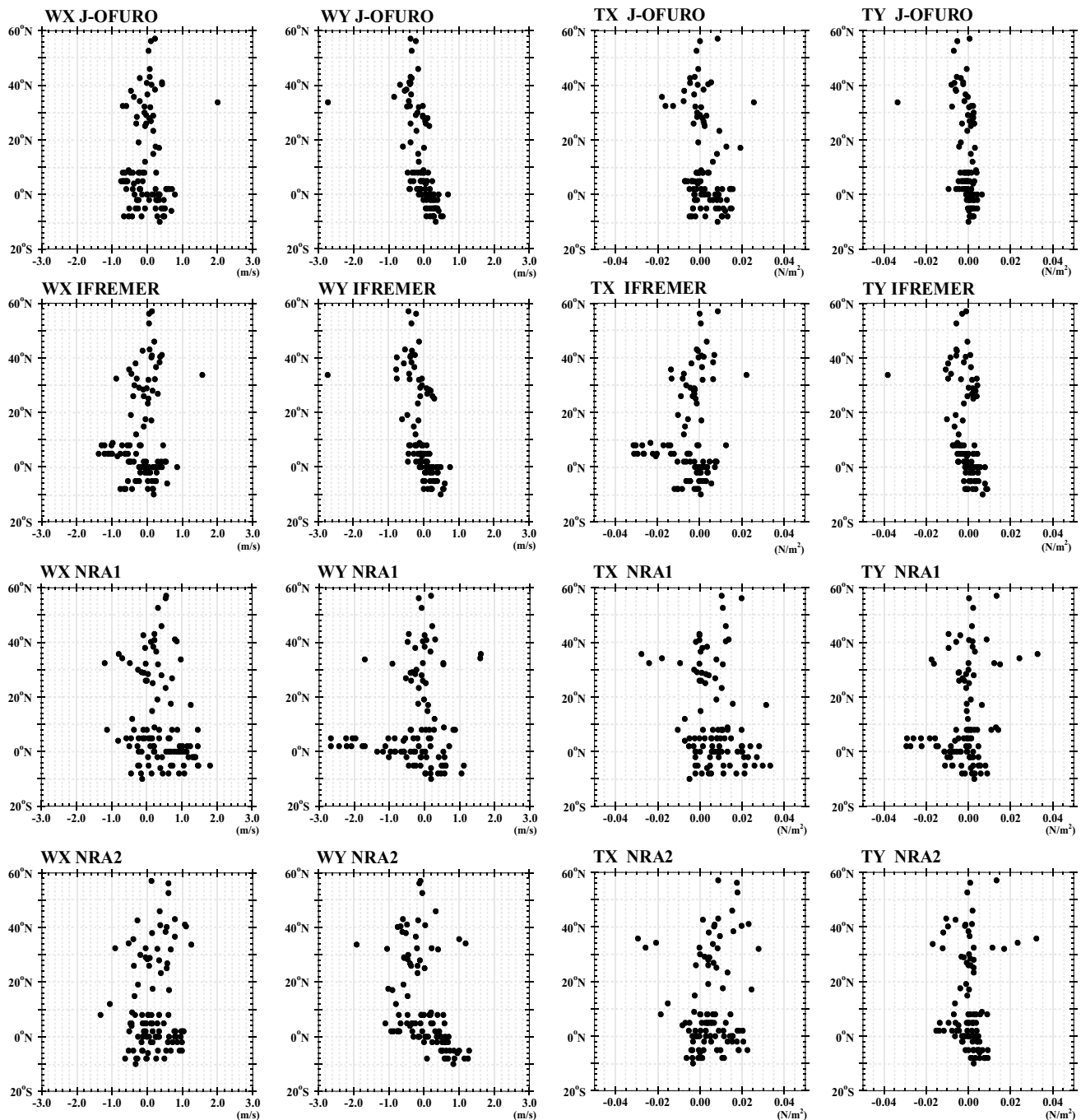
Fig. 4 Scatter plot of the mean difference (MD) among buoy data for latitude (*first column* is zonal wind, *second column* is meridional wind, *third column* is zonal wind stress, and *fourth column* is meridi-onal wind stress) and data sets (*first line* is J-OFURO v2, *second line* is IFREMER, *third line* is NRA1, and *fourth line* is NRA2) at buoy observation points

(Fig. 4). Note that no similar features were found for the NRA2 product.

Differences between MD values for NRA1 and NRA2 products were observed as well. The MDs for both the zonal and meridional wind components from the NRA1 product had positive values in a zone between 5° and 15°N (Fig. 5e, f), while the MDs for the same components from

the NRA2 product were negative in the same zone, corre-sponding to the North Equatorial Current area (Fig. 5i, j).

In addition, the anomalies in the meridional components for the NCEP products (NRA1 and NRA2) from J-OFURO v2 were positive and negative in the northern and southern hemisphere, respectively (Fig. 5f, h, j, l). These poleward anomalies exhibited no clear latitudinal dependencies.
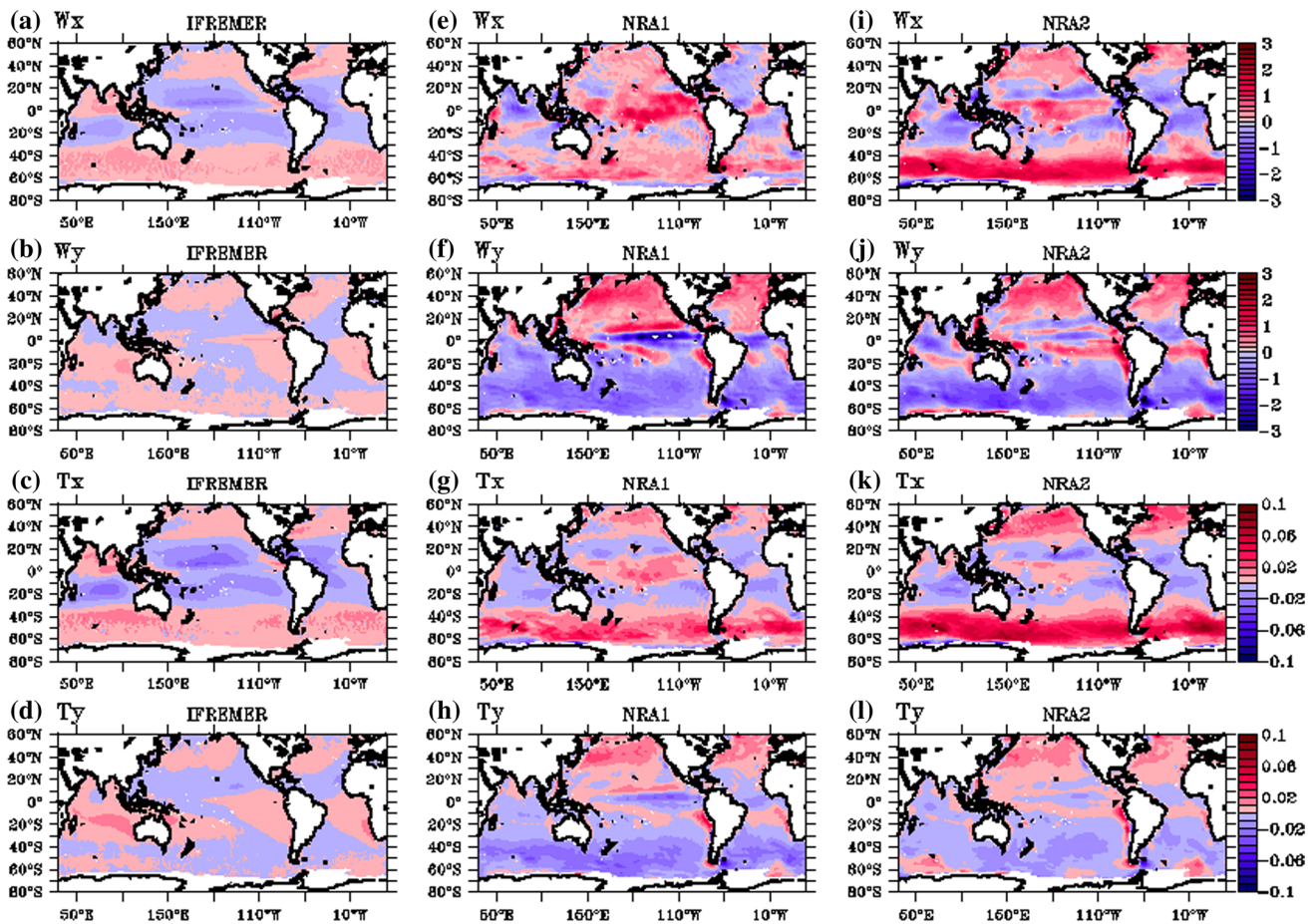
Fig. 5 Mean difference between QSCAT/J-OFURO v2 and other products during 1999/8–2009/7. Zonal wind by **a** IFREMER, **e** NRA1, **i** NRA2. Meridional wind by **b** IFREMER, **f** NRA1, **j** NRA2.

Zonal wind stress by **c** IFREMER, **g** NRA1, **k** NRA2. Meridional wind stress by **d** IFREMER, **h** NRA1, **l** NRA2

Moreover, we also observed fine stripe patterns (with a swath width of approximately 8° and an MD of 0.2 m s^{-1} for zonal wind speed) in the South Pacific in the MD fields of the NCEP products (NRA1 and NRA2) from J-OFURO v2 (Fig. 5e, i). These spatial features were found consistently in the monthly mean fields, suggesting that they were related to data assimilation procedures for the NCEP products. Similar stripe patterns were also found in the wind-stress curl field, which will be discussed in a later section.

3.4 Intercomparison for wind-stress curl field among the data sets

In the previous subsection, we described the differences in the mean values for wind fields derived from different data sets. We expected that these differences would affect the wind-stress curl field, and therefore examined the differences in the meridional profile of the wind-stress curl calculated from different data products. Figure 6 shows the meridional profiles of the wind-stress curl derived from
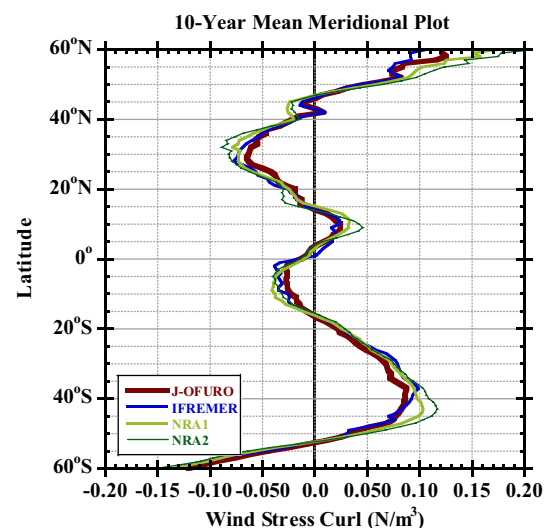
Fig. 6 Meridional profile of decadal mean during 1999/8–2009/7 of wind-stress curl for each data set

10-year averages of the field using four different wind products. The peaks of the wind-stress curl were found at 30°N and 40°S, corresponding to the anticyclonic feature around the subtropical high. The secondary peaks occurring at 10°N and 10°S were related to the cyclonic circulations. The differences for these features were consistent with differences detected in the meridional and zonal wind-stress fields. Large differences for the wind-stress curl were found at latitudes of 30°–35°N with the maximum wind-stress curl reaching 0.03 N m^{-3} (Fig. 6).

We observed differences in wind-stress curl between the J-OFURO and IFREMER data and the reanalysis data (NRA1 and NRA2). Maximum differences in the wind-stress curl were 0.03–0.04 N m^{-3} and occurred in the zone of 40°–50°S. These differences were related to the differences in the meridional profiles of the wind components (Fig. 3), because there were large differences in the meridional profiles of the mean wind fields between the QSCAT and NCEP products in the zone of 40°–45°S.

Other areas with large differences for the wind-stress curl fields based on different products were detected. One area was located at 10°N and 10°S, corresponding to the Northeast and Southeast Trade Wind regions. Another area was located at high latitudes of the southern hemisphere, where the maximum latitude based on the NCEP product (45°S) was clearly different from the value based on the QSCAT product (35°S). While it is difficult to determine which product had a higher reliability, the results suggested that the simulated oceanic flows derived from these wind products would have considerable differences. Note that the wind-stress curl had the smallest magnitude for the J-OFURO v2 product and the largest magnitude for the NRA2 product.

## 4 Validation of time-change indices of wind/ wind-stress fields

4.1 Validation by comparison with in situ measurements from moored buoy observations

In this section, we focus on variations of the wind/wind-stress components over time. The data derived from the J-OFURO v2 products had lower RMSD values and higher correlations for many components than data derived from the other products (Table 1). Differences were observed between the J-OFURO and IFREMER products, even though both are based on the same satellite measurements (QSCAT/SeaWinds). RMSD values were lower for data from J-OFURO v2 than for data from IFREMER. This means that the reliability of satellite-derived wind products can be improved by the data processing procedure.

As suggested in the preceding section, the statistical values in Table 1 were affected considerably by those in the tropical Pacific, because there were many buoys in the low latitudes, especially in the tropical Pacific. In fact, the values in Table 1 are almost the same as those in Table 3. Values of RMSD and R supported the results from the discussion of the mean difference showing that the J-OFURO product has the highest reliability. Further, we found that the NRA2 product has tendencies of low correlations and large RMSDs in the mid-latitude areas (Table 2). In contrast, the IFREMER product has large RMSD for the zonal wind component in the low-latitude areas (Table 3). As the regional dependencies of the statistical comparison were observed again in the time–space change indices, we will survey the latitudinal distribution of the RMSDs at the individual buoy comparisons as in Sect. 3.

Figure 7 shows scatter plots of the RMSD for data from buoy locations for different latitudes. The RMSDs exhibited increasing tendencies with increasing latitude. Certain characteristic features were observed in the equatorial buoy locations (10°N–10°S). For example, the zonal components of the wind and wind stress for the IFREMER product had RMSD values exceeding 3.0 m s^{-1} and 0.04 N m^{-2}, which was consistent with the results for the equatorial Pacific (Table 3). Focusing on the time series in these buoy stations (147°E, 2°N and 5°N, 180°), we observed that the IFREMER wind components exhibited abrupt changes in daily data, which were not found in the time series from other products (Fig. 8a, b). Since these buoy stations with high RMSDs are located in the Australian monsoon trough and the Inter-Tropical Convergence Zone (ITCZ), it is suggested that these high RMSDs were related to errors in satellite-derived wind data caused by rain effects. Such irregular features were not observed in the J-OFURO product. It is possibly because data with high rain probability were removed from the QSCAT swath data in the construction procedure of the J-OFURO product (see Sect. 2.1.1).

The meridional wind speeds for the NRA 1 and NRA2 products had high RMSDs with values greater than 2 m s^{-1} at buoy stations in the equatorial zone (10°N–0°) north of the equator, comparable to data at buoy stations in the mid-latitude areas. No similar features were found in the time series data for the meridional wind-stress components. In fact, the time series at the TAO buoy station (5°N, 140°W) had a high RMSD value (Fig. 8c), and the wind components from NRA1 and NRA2 had significant differences compared to data from the TAO buoy station. Note that this station was selected because there are few missing data. This indicated that data products from NRA2 and NRA1 would be less reliable in this area.
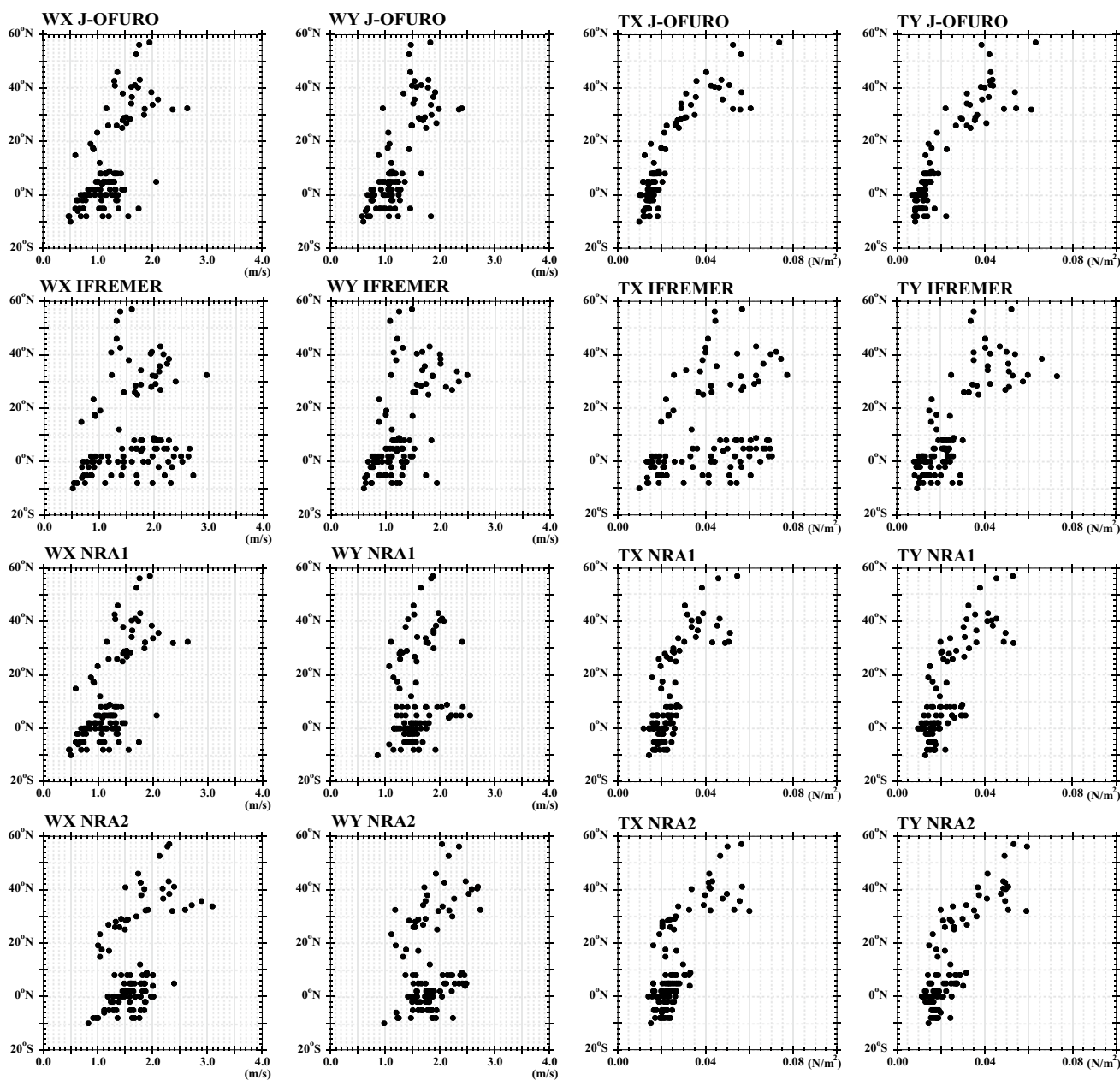
Fig. 7 Scatter plot of the root-mean-square difference (RMSD) among buoy data for latitude (*first column* is zonal wind, *second column* is meridional wind, *third column* is zonal wind stress, and *fourth column* is meridional wind stress) and data sets (*first line* is J-OFURO v2, *second line* is IFREMER's, *third line* is NRA1, and *fourth line* is NRA2) at buoy stations

4.2 Intercomparison of variations in wind field among the data sets

We calculated correlation coefficients and RMS differences for each grid point in each data set referred to the QSCAT/ J-OFURO v2 product to determine whether there were differences in time variations among the data sets (Figs. 9, 10). The correlation coefficients between the J-OFURO and other data sets had no negative values, indicating that the time variations were similar among the data sets. We can recognize some discrepancies from the J-OFURO which were already mentioned in the preceding section: the difference in IFREMER zonal component in the Pacific equatorial zone near ITCZ as well as the wind stress (Figs. 9a, c, 10a, c), and that in NCEP meridional component in the low-latitude areas.

Closely looking at the correlation coefficients for the NCEP product in the Pacific low latitudes (Fig. 9f, j, h, l), we found a zonal structure with high and low correlation coefficients in the areas. The correlations were very low in

(a)

(b)

(c)
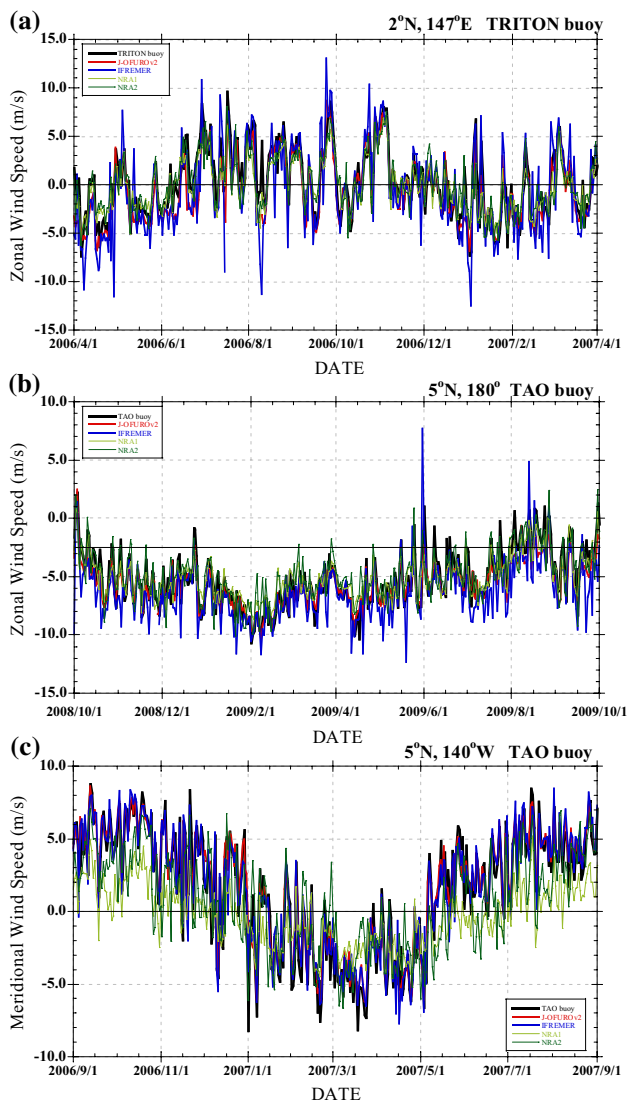
Fig. 8 Time series of wind components by TAO/TRITON buoy and data sets: **a** zonal wind at 2°N, 147°E; **b** meridional wind at 5°N, 140°W; **c** zonal wind at 5°N, 180°

the equatorial band, relatively high to the north of it, and again low in a zonal band corresponding to the mean position of ITCZ near 10°N. In contrast, the RMSD showed relatively high values in the zone with relatively high correlation coefficients (Fig. 10f, j, h, l). The difference tended to increase from summer to winter (Fig. 8c). In the area near the ITCZ, it is suggested that the differences were also caused by the different spatial resolutions of the data sets as well as the rainfall effects. Further, we expect that short-term variations on a time scale of a few days also influence the RMSD. Note that the distribution of correlation coefficients between the NCEP and J-OFURO products exhibited stripe patterns in the equatorial zone (Fig. 9e–l), while no such patterns were observed in the comparison between the

IFREMER and J-OFURO products. The stripe patterns in the RMSDs for the wind components approached 1 m s^{-1} in magnitude with a swath width of approximately 15°. More details will be discussed in Sect. 5.

In addition, large RMSDs of the NCEP products were found in the mid- and high-latitude areas corresponding to the subarctic oceans, especially in the Antarctic Ocean (Fig. 10). This was not evident in the IFREMER products (Fig. 10a–d). This might be attributed to a low reliability for the satellite wind products as a result of sea ice, and could be verified by comparisons with in situ measurements from mooring buoys in the Antarctic Ocean.

5 Discussion

We found some serious discrepancies between the J-OFURO and other products (IFREMER and NCEP ones) in low latitudes of the Pacific, possibly due to the construction procedures used for them. In this section, we will discuss the problems in more detail. First, we notice a problem for the IFREMER product in our results. We observed several discrepancies among the products when examining the time series of wind components at the TAO buoy station in the equatorial Pacific Ocean (8°N, 95°W) (Fig. 11a). In particular, the time series from the IFREMER product had spike signals that were also evident in other time series (Figs. 8a, b). Compared with data from other buoy stations, relatively large differences among the data sets were found in the time series of the TAO buoy station (8°N, 95°W). Even though both the J-OFURO and the IFREMER products are derived from QSCAT data, no similar spike signals were found in the time series data from the J-OFURO product. This meant that spike signals had been removed during the data conversion process using the weighted average method (Kutsuwada 1998). Thus, when comparing time series data from the J-OFURO and IFREMER products, we observed spike signals that were random and had no clear time dependence.

Regarding this problem, our analyses also included the newer product IFREMER v3, which was developed using the new L2B v3 data and the same method as for the IFREMER v2 product. Time series of the wind speed and direction were compared between the two IFREMER products, v2 and v3 (Fig. 11b, c). We did not observe spike signals in the wind speed in the time series data from the newest IFREMERv3 product (Fig. 11b). These results suggested that the spike signals might have been caused by errors in the QSCAT L2B v2 product, and many of these errors were removed in the construction procedure of the J-OFURO v2 product. In fact, in the L2Bv3 data, such errors had been minimized (Fore et al. 2014). Further, the comparison between time series of the wind direction (Fig. 11c)
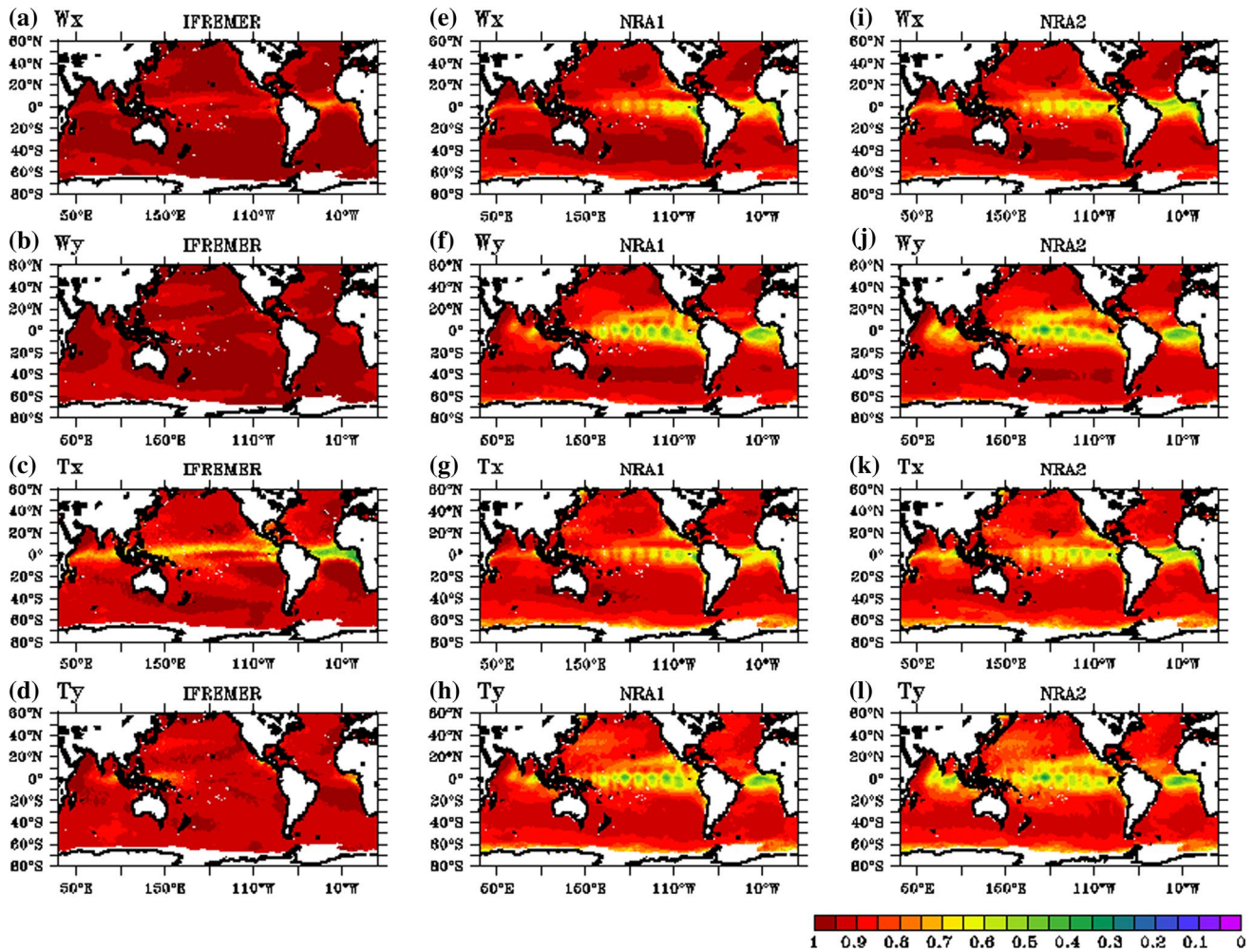
Fig. 9 Correlation coefficients between J-OFURO and other data sets for wind components during 1999/8–2009/7. Zonal wind by **a** IFREMER, **e** NRA1, **i** NRA2. Meridional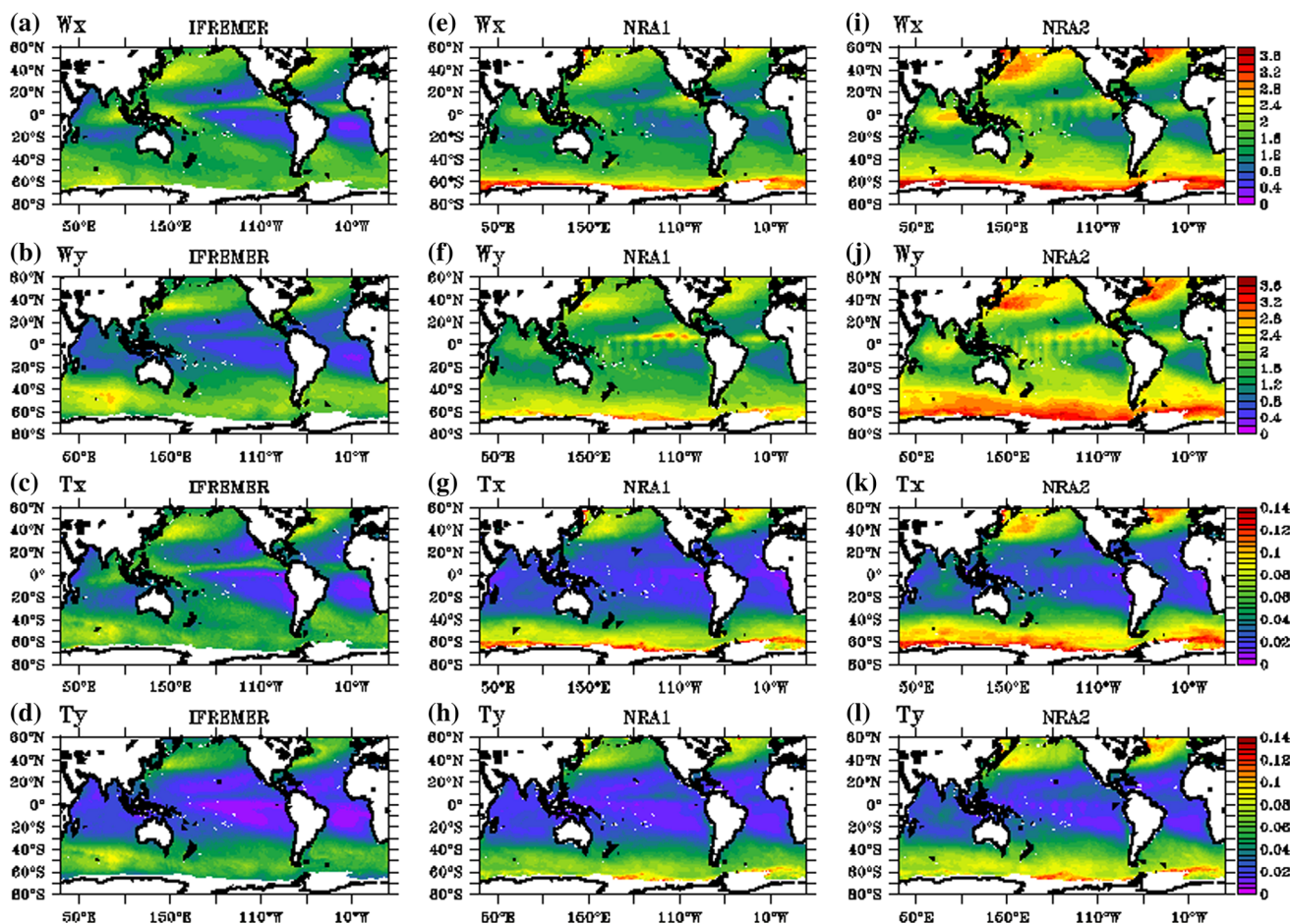 wind by **b** IFREMER, **f** NRA1, **j** NRA2. Zonal wind stress by **c** IFREMER, **g** NRA1, **k** NRA2. Meridional wind stress by **d** IFREMER, **h** NRA1, **l** NRA2

revealed that no spike signals were found. Therefore, it was assumed that the QSCAT L2B v2 data had significant errors due to rain effects, resulting in the spike noise in the IFREMER v2 product.

Next, we focus on problems for the NCEP products in the equatorial Pacific. We found large differences in the MDs and RSMDs for wind fields in the equatorial ocean (Figs. 5, 9, 10). Stripe patterns were found in the equatorial Pacific Ocean for the correlation coefficient, the MD, and the RMSD when comparing the NCEP (NRA1 and NRA2) and the J-OFURO data products. No such patterns were found in the equatorial areas of the Atlantic and Indian Oceans. Since there are TAO/TRAITON buoy stations in the equatorial Pacific Ocean (Fig. 1), we can perform additional validations using the buoy observation data.

The statistical values for the TAO/TRITON data (Table 3) revealed that the J-OFURO v2 product had a higher reliability than the NCEP products (NRA1 and

NRA2). This suggests that the stripe patterns shown in Figs. 5, 9, and 10 might have been caused by data conversion procedures for the NCEP products (NRA1 and NRA2). With regard to this issue, we observe spatial features associated with the correlations between the J-OFURO v2 and NRA1 products near the TAO buoy stations in the equatorial Pacific (denoted by stars in Fig. 12). It was evident that the stripe pattern was associated with the buoy locations. The correlation coefficients had lower values in areas between the buoy stations and higher values close to the stations. The striped features also occurred in the MD and RMSD fields as well as for the correlations for the wind and wind-stress components in the comparison of the NCEP products (NRA1 and NRA2) and the J-OFURO v2 product. Because the reliabilities for satellite-derived wind products do not depend on buoy locations, it is assumed that the observed spatial features occurring near the buoy locations were due to data assimilation and conversion

Fig. 10 Root-mean-square difference (RMSD) between the QSCAT/ J-OFURO and other products during 1999/8–2009/7. Zonal wind by **a** IFREMER, **e** NRA1, **i** NRA2. Meridional wind by **b** IFREMER, **f** NRA1, **j** NRA2. Zonal wind stress by **c** IFREMER, **g** NRA1, **k** NRA2. Meridional wind stress by **d** IFREMER, **h** NRA1, **l** NRA2

procedures for the NCEP reanalysis products. Similar spatial features in the numerical product were detected in a previous study (Tomita and Kubota 2006), which showed a spatial distribution of the specific humidity of the sea surface using a different product (ECMWF reanalysis). The authors suggested that the spatial features were artificial and likely due to a problem in the assimilation procedure of the numerical model.

The surface data in the NCEP reanalysis products were developed using an optimum interpolation method incorporating forecast data and measurement data (Kalnay et al. 1996). Thus, the spatial features (Fig. 12) suggested that the forecasted surface data based on the NCEP product should not have any issues in the equatorial regions. If the forecasted data contained errors, they would be minimized in areas around measurement locations such as the buoy stations. In the equatorial Pacific where there is a buoy array, we would expect fewer errors in the forecasted data near the buoy stations, but not in other areas if the errors were due to the assimilation procedure. These

errors would result in the stripe features in the equatorial Pacific. On the other hand, stripe features were less obvious in the equatorial Atlantic as a result of fewer buoy stations.

In addition, we noticed spatial features in the daily mean wind vector field in summer (Fig. 13) and winter (Fig. 14) for the NCEP products. In the equatorial Pacific, wind speeds were lower for the NRA1 product than for the J-OFURO v2 product, and the meridional gradients of the wind direction were stronger for the J-OFURO v2 than the NRA1 products. In the J-OFURO v2-derived wind field of December 15, 2002 (indicated by a red box in Fig. 14), we observed weak westerly winds and a divergent feature in an area around 2°S and 180°–140°W, but these features were not as clear in the NRA1 product. We found similar features for August 15, 2002 in the areas of 2°N–2°S and 160°E–160°W (indicated by a red box in Fig. 13), but there were differences between the two wind fields. These indicated that the J-OFURO v2 product had more detailed features than the NRA1 product.

In a comparison between the NRA2 and the J-OFURO v2 wind fields, spatial changes in the wind direction were better defined in the NRA2 product than in the J-OFURO v2 product. For example, the weak wind structure was
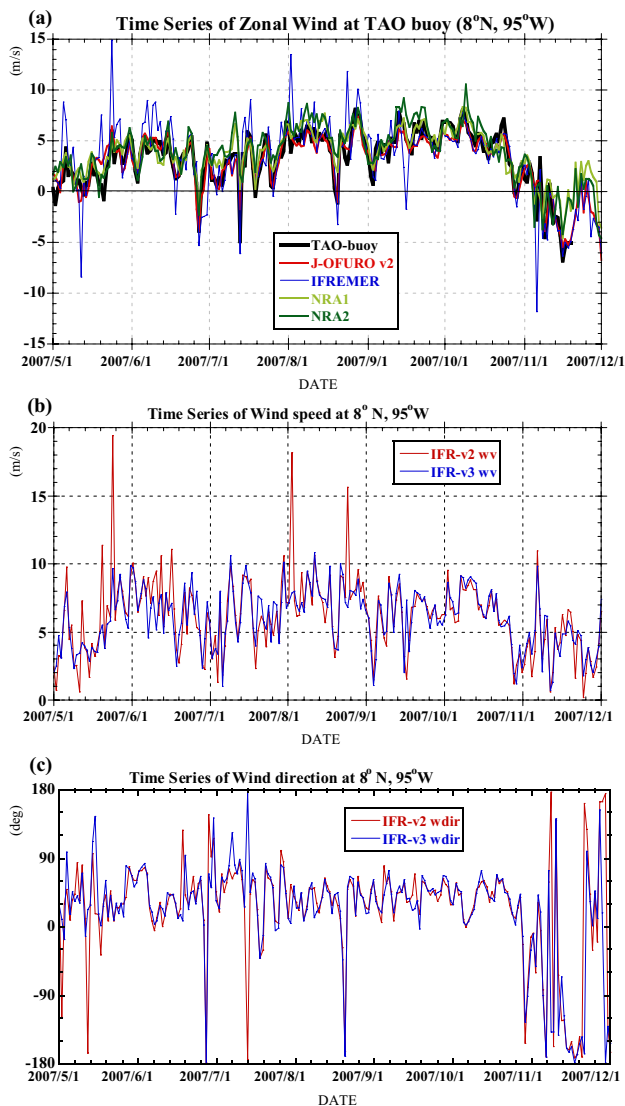
Fig. 11 Time series of the zonal wind **a** at TAO buoy station at 8°N, 95°W for four different wind products and buoy measurements, wind speed (**b**) and wind direction (**c**) for IFREMER v2 and v3 products
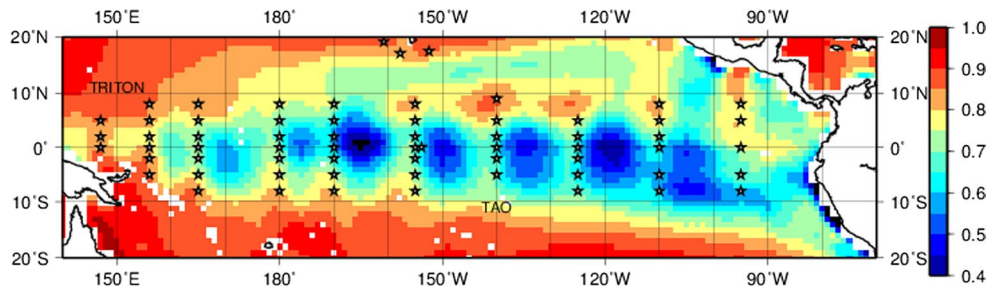
clearly different for the NRA2 and J-OFURO products on August 15, 2002, in the areas 5°N–20°S and 140°E–160°W (indicated by a blue box in Fig. 13). In the Westerlies region (30°N–50°N and 130°W–160°W) of the North Pacific in winter, we detected the two maxima of the westerly winds in the NRA2 wind field, but this feature was less clear in the J-OFURO v2 product (indicated by a blue box in Fig. 14). This indicated that the J-OFURO wind field contained less information with regard to small details than the wind field derived from NRA2. The validations based on comparisons with the buoy measurements demonstrated that the reliabilities of the wind fields were higher for the J-OFURO v2 product than for the NRA1 and the NRA2 products. Thus, the above results suggested that the NRA1 product resulted in a smoother output than the NRA2 product. These discrepancies may have caused the difference in the calculation results of the air–sea coupled model driven by wind data. In addition, the different features between the NRA1 and NRA2 products have been pointed out as the equatorial divergent winds by Kanamitsu et al. (2002).

6 Summary

In this study, we have performed validation for the QSCAT/ J-OFURO v2 data based on buoy observations data for a decade and investigated the reliabilities of major wind vector data sets (QSCAT/IFREMER, NRA1 and NRA2) by examining differences among the wind data sets.

In the first step, we have validated the mean fields for the data sets. The reliabilities of mean fields are important for the wind-stress curl, which is calculated using the mean wind-stress vector field. Thus, we compared the 10-year mean fields among the data sets. The results showed that the differences among data sets were spatially related to the westerly and trade wind regions. Next, we validated the mean fields by comparisons with in situ measurements from moored buoy observations. The features for the mean differences were dissimilar for all the buoy data compared to the buoy data at the low- and mid-latitude areas. For example, the meridional wind component from the NRA2 product had relatively low MD values for all buoys (Table 2), but positive and negative MD values were found
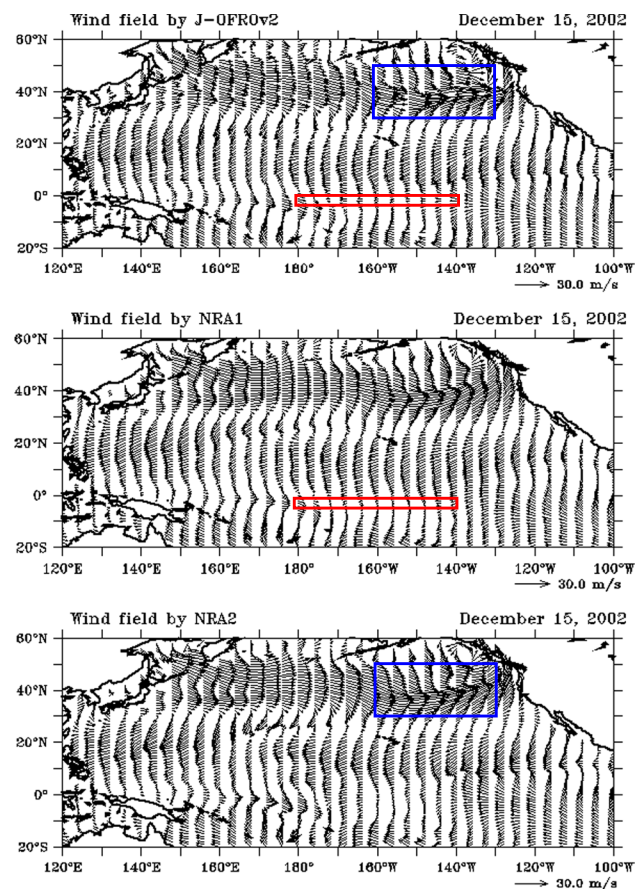

Fig. 12 Correlation coefficients (*color*) between J-OFURO v2 and NRA1 for meridional wind during 1999/8–2009/7 at buoy station (*star*). (Color figure online)
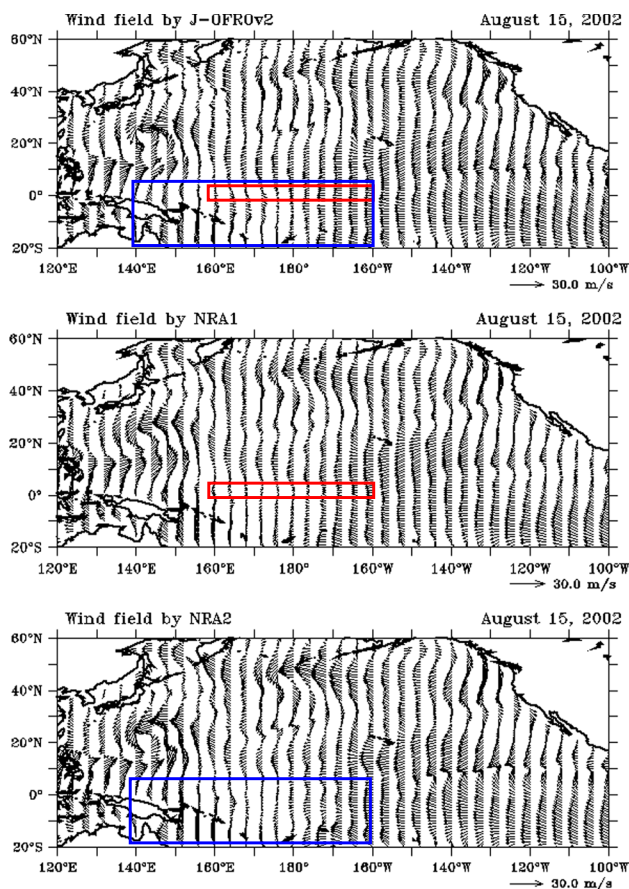
Fig. 13 Wind vector field on August 15, 2002 from J-OFURO v2 (*upper*), NRA1 (*middle*), and NRA2 (*lower*). *Red* and *blue boxes* indicate focus regions (see text). (Color figure online)

Fig. 14 Wind vector field on December 15, 2002 from J-OFURO v2 (*upper*), NRA1 (*middle*), and NRA2 (*lower*). *Red* and *blue boxes* indicate focus regions (see text). (Color figure online)

for individual buoy stations. This suggested that the large MD values with different signs canceled each other out in the zonal averages. Improving the accuracy would require one to calculate the MDs at each buoy station or determine regional means. In addition, the MDs at buoy stations in the equatorial zone were higher for some products than for the J-OFURO v2.

For areas with few buoy stations, we calculated the MDs for other products from the QSCAT/J-OFURO-derived wind fields. Large MDs were found in the equatorial zone (between 20°N and 20°S) and in the westerlies region (near 40°N/S), suggesting that the differences among data sets were affected by the location of the westerlies and the trade winds. Those differences were likely caused by the resolvability of the phenomenon and the different grid sizes of the data sets.

We detected positive MDs for the wind components in near-coastal regions within approximately 5° of the west coast of North and South America. These features were related to the large negative MDs derived from the gridded QSCAT product at coastal buoy stations in the zone of 30°N–40°N (Fig. 8), suggesting that the gridded satellite data contained errors in near-coastal regions. Further, the MDs for the J-OFURO v2 product had relatively large values in the equatorial areas, especially in the central equatorial Pacific (150°E–110°W).

Since those differences in MD were related to the differences in the wind-stress curl fields among the data sets, we investigated the differences in the meridional profile of the wind-stress curl. Differences were detected in areas with large wind-stress curl, and those differences among the data sets were 0.03 N m^{-2} in the zones of 30–35°N and 40–45°N (Fig. 4). Differences in the wind-stress curl among the data sets can result in differences in wind-driven current (Aoki and Kutsuwada 2008).

In addition, we validated the time changes in the fields for all data sets. The statistical values using all the buoy data exhibited the same features using low-latitude and mid-latitude buoy data. However, statistical values for the IFREMER and NCEP products had low reliabilities in the equatorial zone. The RMSDs were different among the buoy stations of the latitude band in many buoy stations

(30–40°N and 10°N–10°S). In the equatorial region, the wind components for the IFREMER and NCEP products had high RMSDs, suggesting that they contained errors. Specifically, there were spike noises in the time series for the IFREMER product, suggesting that the noise was caused by rain effects (Fore et al. 2014)

We validated the time changes in wind fields for the data sets based on the J-OFURO v2 product. Differences among the data sets were observed in the low-latitude zone at 130°E–70 W° and 5°N–10°N, and those differences were associated with the ITCZ. Further, in the equatorial Pacific, we detected stripe patterns (10°N–10°S) in the distribution of the RMSD between the NCEP and J-OFURO products. We focused on stripe patterns in the equatorial Pacific Ocean, where relatively low correlation coefficients were found when comparing the NCEP products (NRA1 and NRA2) and the J-OFURO v2 product. This stripe pattern was characterized by higher correlations around buoy stations and lower correlations away from buoy stations. The J-OFURO v2 product had relatively higher reliability than the NRA1 and NRA2 products, suggesting that the problems were associated with data assimilation and conversion procedures of the gridded data.

References

Aoki K, Kutsuwada K (2008) Verification of the wind-driven transport in the North Pacific subtropical gyre using gridded wind-stress products. J Oceanogr 64(1):49–60

Bentamy A, Queffeulou P, Quilfen Y, Graima N, Lenaourand M, Servain J (1996) Determination and validation of average wind fields from ERS-1 scatterometer measurements. Glob Atmos Ocean Syst 4:1–29

Bentamy A, Grodsky SA, Chapron B, James CA (2014) Compatibility of C- and Ku-band scatterometer winds: ERS-2 and QuikSCAT. J Mar Syst 117:72–80. doi:10.1016/j.jmarsys.2013.02.008

Chelton DB, Schlax MG, Freilich MH, Milliff RF (2004) Satellite measurements reveal persistent small-scale features in ocean winds. Science 303:978–983

Fairall CW, Bradley EF, Rogers DP, Edson JB, Young GS (1999) Bulk parameterization of air-sea fluxes for TOGA-COARE. J Geophys Res 101:3747–3764

Fore AG, Stiles BW, Chau AH, Williams B, Dunbar RS, Rodriguez E (2014) Point-wise wind retrieval and ambiguity removal improvements for the QuikSCAT climatological data set. Geosci Remote Sens IEEE Trans 52(1):51–59

Kalnay EM et al (1996) The NCEP/NCAR 40-year reanalysis is project. Bull Am Meteorol Soc 77:437–471

Kanamitsu M, Ebisuzaki W, Woollen J, Potter P, Fiorion M (2002) NCEP/DOE AMIP-II reanalysis (R-2). Bull Am Meteorol Soc 83:1631–1643

Kubota M, Iwasaka N, Kizu S, Konda M, Kutsuwada K (2002) Japanese ocean flux data sets with use of remote sensing observations (J-OFURO). J Oceanogr 58(1):213–225

Kutsuwada K (1998) Impact of wind/wind-stress field in the North Pacific constructed by ADEOS/NSCAT data. J Oceanogr 54:443–456

Kutsuwada K, Kasahara M, Aoki K (2004) Gridded surface wind-stress product over the world ocean constructed by satellite scatterometer data and its comparison with NWP products. Proc PORSEC 2004 68(2):348–354

Kutsuwada K, Koyama M, Morimoto N (2009) Validation of gridded surface wind products using space borne microwave sensor s and their application to air-sea inter action in the Kuroshio Extension region. J Remote Sens Soc Jpn 29(1):1–12

Large WG, Pond S (1981) Open ocean momentum flux measurements inmoderate to strong winds. J Phys Oceanogr 11:324–336

Liu WT, Katsaros KB, Businger JA (1979) Bulk parameterization of air-sea exchanges of heat and water vapor including the molecular constraints at the interface. J Atmos Sci 36:1722–1735

Risien MC, Chelton DB (2008) A global climatology of surface wind and wind stress fields from eight years of quikscat scatterometer data. J Phys Oceanogr 38:2379–2413

Sasaki H, Nonaka M (2006) Far-reaching Hawaiian Lee Countercurrent driven by wind-stress curl induced by warm SST band along the current. Geophys Res Lett 33(13):L13602. doi:10.1029/2006GL026540

Sasaki H, Sasai Y, Nonaka M, Masumoto Y, Kawahara S (2006) An eddy-resolving simulation of the quasi-global ocean driven by satellite-observed wind field: preliminary outcomes from physical and biological fields. J Earth Simul 6:35–49

Small RJ, deSzoeke SP, Xie SP, O'Neill L, Seo H, Song Q, Cornillon P, Spall M, Minobe S (2008) Air-sea interaction over ocean fronts and eddies. Dyn Atmos Ocean 45:274–319

Smith SD (1980) Wind-stress and heat flux over the ocean the ocean in gale force winds. J Phys Oceanogr 10:709–726

Sverdrup HU (1947) Wind-driven cur rents in a baroclinic ocean with application to the equatorial currents of the eastern Pacific. Proc Natl Acad Sci USA 33:318–326

Tomita H, Kubota M (2005) Increase in turbulent heat flux during the 1990s over the Kuroshio/Oyashio Extension region. Geophys Res Lett 32:L09705. doi:10.1029/2004GL022075

Tomita H, Kubota M (2006) An analysis of the accuracy of Japanese ocean flux data sets with use of remote sensing observations (J-OFURO) satellite-derived latent heat flux using moored buoy data. J Geophys Res 111:C07007. doi:10.1029/2005JC003013

Wunsch C (1998) The work done by the wind on the oceanic general circulation. J Phys Oceanogr 28:2332–2340

Xie S-P (2004) Satellite observations of cool ocean-atmosphere interaction. Bull Am Meteorol Soc 85:195–208